Inorg. Chem. **2007**, *46*, 1459–1463

Crystal Structure, Electronic Structure, and Physical Properties of $Ti_{1-\delta}Mo_{1+\delta}As_4$ and $Ti_{1-\delta}Mo_{1+\delta}Sb_4$

Shahab Derakhshan, Abdeljalil Assoud, Katja M. Kleinke, and Holger Kleinke*

Department of Chemistry, University of Waterloo, Waterloo, Ontario, N2L 3G1 Canada

Received October 9, 2006

The new ternary pnictides, $Ti_{1-\delta}Mo_{1+\delta}Pn_4$ (Pn = As, Sb), were uncovered during our search for novel thermoelectric materials. Both compounds crystallize in the $OsGe_2$ type in the monoclinic space group *C*2/*m*, with lattice dimensions of $a = 10.1222(9)$ Å, $b = 3.6080(3)$ Å, $c = 8.1884(8)$ Å, $\beta = 120.230(2)°$, and $V = 258.38(7)$ Å^3 ($Z = 2$) for $Ti_{0.79(1)}Mo_{1.21}Sb_4$ and $a = 9.1580(2)$ Å, $b = 3.3172(1)$ Å, $c = 7.6666(1)$ Å, $\beta = 119.496(1)°$, and $V = 202.720(4)$ Å^3 ($Z = 2$) for $Ti_{0.86(2)}Mo_{1.14}As_4$. The electronic structure calculations predicted metallic behavior for these compounds, which was in agreement with the measured temperature dependence of the electrical conductivity and Seebeck coefficient.

Introduction

Thermoelectric materials are able to convert thermal energy into electricity (Seebeck effect) and vice versa (Peltier cooling). Promising materials are narrow band gap semiconductors composed of heavy elements and complex crystal structures.[1,2] These include heavy main group element compounds such as $CsBi_4Te_6$[3] or the filled skutterudites, i.e., $LaCoFe_3Sb_{12}$,[4] that contain late transition metal atoms.

Since the late 1990s our research group has investigated early transition metal antimonides. Initially, we focused on the metal-rich part of the respective phase diagrams with M/Sb ratios ≥ 1.[5−13] These materials are composed of heavy elements and exhibit complex crystal structures of high symmetry including mixed occupancies and (rarely) rattling atoms as well as high thermal stabilities. Therefore, aside from their metallic properties, they would be ideal candidates for thermoelectric applications. Subsequently, we turned our attention toward the Sb-rich region[14−17] to find nonmetallic materials.

In contrast to the late transition metal antimonides, which usually have band gaps within the d states of the metals (as in the skutterudites, namely, between the t_{2g} and e_g states), all known early transition metal antimonides are metallic. To illustrate this, the densities of states (DOS) of selected examples with low M/Sb ratios are presented in Figure 1.

In all of these selected binaries, the lowest occupied states are antimony s (below the energy window shown) and p states, which dominate the area between the Fermi level (fixed at 0 eV) and −6 eV. The local minima in the vicinity of the Fermi levels typically result from an overlap of the metal d dominated peak with the antimony p peak. Among these examples, Mo_3Sb_7[18] is the only one that exhibits a band gap. However, since the gap is located above the Fermi level, Mo_3Sb_7 is metallic. This compound was rendered semiconducting by partial replacement of antimony by tellurium atoms, leading to $Mo_3Sb_{5+\delta}Te_{2-\delta}$, which exhibits promising thermoelectric properties.[19] In fact, $Mo_3Sb_{5.4}Te_{1.6}$ is one of the leading high-temperature thermoelectrics.[20]

* To whom correspondence should be addressed. E-mail: kleinke@uwaterloo.ca.

(1) Rowe, D. M. *CRC Handbook of Thermoelectrics*; CRC Press: Boca Raton, FL, 2006.
(2) Ioffe, A. F. *Physics of Semiconductors*; Academic Press: New York, 1960.
(3) Sales, B. C.; Mandrus, D.; Williams, R. K. *Science* **1996**, *272*, 1325.
(4) Chung, D.-Y.; Hogan, T.; Brazis, P.; Rocci-Lane, M.; Kannewurf, C.; Bastea, M.; Uher, C.; Kanatzidis, M. G. *Science* **2000**, *287*, 1024.
(5) Kleinke, H. *Chem. Commun.* **1998**, 2219.
(6) Kleinke, H. *J. Mater. Chem.* **1999**, *9*, 2703.
(7) Kleinke, H. *Inorg. Chem.* **1999**, *38*, 2931.
(8) Kleinke, H. *J. Am. Chem. Soc.* **2000**, *122*, 853.
(9) Kleinke, H. *Chem. Soc. Rev.* **2000**, *29*, 411.
(10) Kleinke, H.; Ruckert, C.; Felser, C. *Eur. J. Inorg. Chem.* **2000**.
(11) Bobev, S.; Kleinke, H. *Chem. Mater.* **2003**, *15*, 3523.
(12) Derakhshan, S.; Assoud, A.; Kleinke, K. M.; Dashjav, E.; Qiu, X.; Billinge, S. J. L.; Kleinke, H. *J. Am. Chem. Soc.* **2004**, *126*, 8295.
(13) Kleinke, H. *Eur. J. Inorg. Chem.* **1998**, 1369.
(14) Assoud, A.; Kleinke, K. M.; Soheilnia, N.; Kleinke, H. *Angew. Chem., Int. Ed.* **2004**, *43*, 5260.
(15) Kleinke, H. *Inorg. Chem.* **2001**, *40*, 95.
(16) Elder, I.; Lee, C.-S.; Kleinke, H. *Inorg. Chem.* **2002**, *41*, 538.
(17) Soheilnia, N.; Assoud, A.; Kleinke, H. *Inorg. Chem.* **2003**, *42*, 7319.
(18) Brown, A. *Nature* (*London*) **1965**, *206*, 502.
(19) Dashjav, E.; Szczepenowska, A.; Kleinke, H. *J. Mater. Chem.* **2002**, *12*, 345.
(20) Gascoin, F.; Rasmussen, J.; Snyder, G. J. *J. Alloys Compd.*, in press.

10.1021/ic0619254 CCC: $37.00
Published on Web 01/18/2007

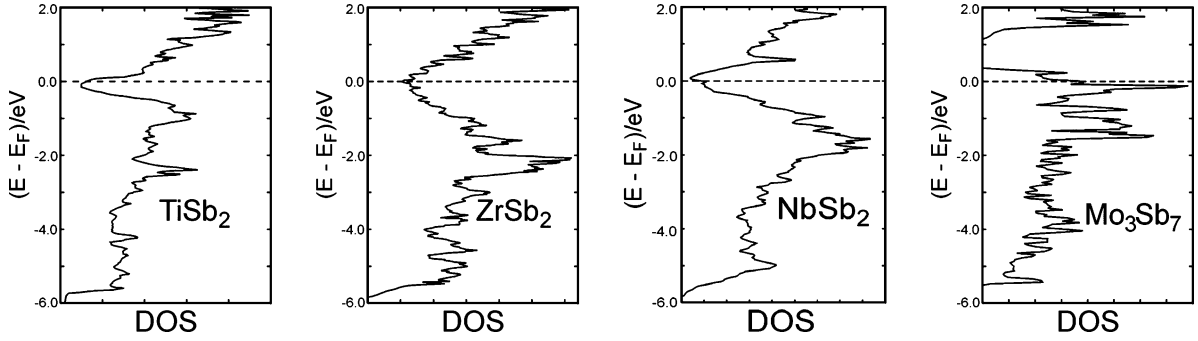

Figure 1. The DOS of selected early transition metal antimonides. The horizontal dashed lines denote the Fermi levels, arbitarily placed at 0 eV.

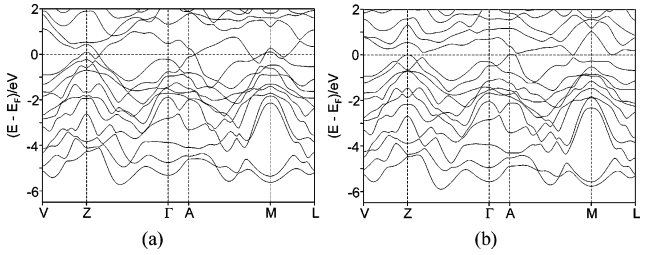

Figure 2. The electronic structure of $NbSb_2$ (a) and $HfMoSb_4$ (b). The horizontal dashed lines denote the Fermi levels, arbitarily placed at 0 eV.

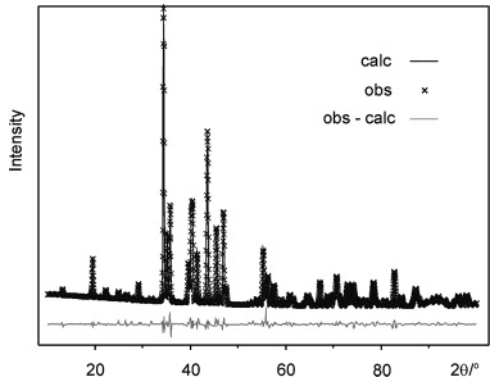

Figure 3. Rietveld refinement of the experimental X-ray powder data of $TiMoAs_4$.

For the other three examples, we considered the possibility of lowering the small residual DOS at the Fermi level and creating small band gap semiconductors by chemical modifications. We began with $NbSb_2$,[21] as it shows the smallest DOS at the Fermi level. Our calculations showed that a few bands of mostly Nb d character cross the Fermi level (E_F, arbitrarily placed at 0 eV in Figure 2a) along several directions. These bands exhibit steep slopes at E_F leaving low electron density at Γ. We proposed that polarizing the M−M interactions would avoid these band crossings, which led to the discovery of the first nonmetal early transition metal antimonide, $HfMoSb_4$. The electronic structure calculation for $HfMoSb_4$ (Figure 2b) predicted semimetallic behavior for this material, which was subsequently proven by experiment.[22]

Furthermore, we decided to examine isostructural systems with the different M pairs. In this paper we present the results of our investigations in the systems Ti/Mo/As and Ti/Mo/Sb.

(21) Rehr, A.; Kauzlarich, S. M. *Acta Crystallogr., Sect. C* **1994**, *50*, 1177.
(22) Derakhshan, S.; Kleinke, K. M.; Dashjav, E.; Kleinke, H. *Chem. Commun.* **2004**, 2428.

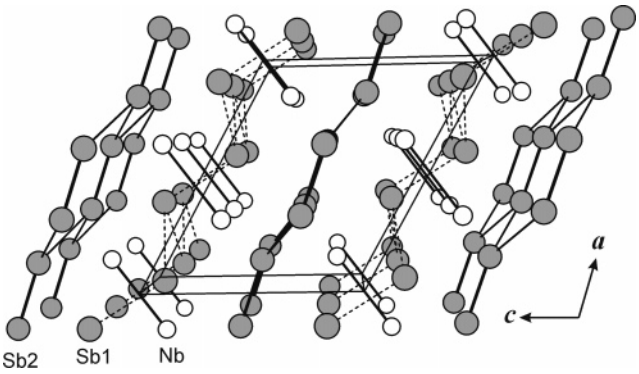

Figure 4. Projection of the crystal structure of $NbSb_2$ along [010]; white circles, Nb; gray circles, Sb.

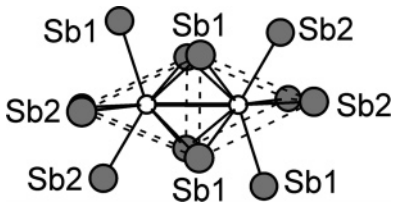

Figure 5. Two bicapped trigonal prisms of $NbSb_8$, condensed via the common rectangular face. The dashed lines indicate the edges of the trigonal prisms.

Table 1. Crystallographic Data for $Ti_{0.8}Mo_{1.2}Sb_4$ and $Ti_{0.9}Mo_{1.1}As_4$

empirical formula	$Ti_{0.79(1)}Mo_{1.21}Sb_4$	$Ti_{0.86(2)}Mo_{1.14}As_4$
fw (g/mol)	641.17	450.22
T (K)	298(2)	298(2)
wavelength (Å)	0.71073	1.5406
space group	*C*2/*m*	*C*2/*m*
a (Å)	10.1222(9)	9.1580(2)
b (Å)	3.6080(3)	3.3172(1)
c (Å)	8.1884(8)	7.6666(1)
β (deg)	120.230(2)	119.496(1)
V (Å^3)	258.38(7)	202.720(4)
no. of formula units per cell	2	2
calc density (g/cm^3)	8.241	7.38
R1,[a] wR2 (all data)	0.022, 0.050	
Rp,[b] wRp		0.048, 0.053

[a] $R1 = \Sigma||F_o| - |F_c||/\Sigma|F_o|$; $wR2 = [\Sigma[w(F_o^2 - F_c^2)^2]/\Sigma[w(F_o^2)^2]]^{1/2}$. [b] $Rp = \Sigma|y_{obs} - y_{calc}|/\Sigma|y_{obs}|$; $wRp = [\Sigma[w(y_{obs}^2 - y_{calc}^2)^2]/\Sigma[w(y_{obs})^2]]^{1/2}$.

Experimental Section

Syntheses. All samples were prepared from stoichiometric mixtures of the elements (powder form, ALFA Aesar, nominal purities >99.5%). In the Ti/Mo/Sb system, Ti/Mo ratios of 3:6, 4:5, 4.5:4.5, 5:4, and 6:3 were attempted, while keeping the M/Sb ratio at 9:18 = 1:2. The best yield of the $OsGe_2$ structure type was obtained in the 4:5:18 ratio of the elements (i.e., $Ti_{0.89}Mo_{1.11}Sb_4$).

Table 2. Atomic Coordinates, Equivalent Isotropic Displacement Parameters, and Occupancy Factors for $Ti_{0.8}Mo_{1.2}Sb_4$ and $Ti_{0.9}Mo_{1.1}As_4$

	$Ti_{0.8}Mo_{1.2}Sb_4$			$Ti_{0.9}Mo_{1.1}As_4$		
	M	Sb1	Sb2	M	As1	As2
x	0.15193(5)	0.40504(3)	0.34992(3)	0.1566(2)	0.4038(2)	0.3544(2)
y	0	0	$^1/_2$	0	0	$^1/_2$
z	0.19107(7)	0.11178(4)	0.46187(4)	0.1996(2)	0.1065(2)	0.4676(2)
U_{eq}/Å^2	0.0059(2)	0.0070(1)	0.0065(1)	0.0063(8)	0.0263(8)	0.090(8)
occ Ti/Mo	0.397(5)/0.603			0.43(1)/0.57		

The mixture was heated in two steps to 600 and 1000 °C in an open ceramic container placed inside an evacuated fused silica tube. The X-ray powder pattern displayed high yields of the target phase and barely visible traces of side products. Because the reactions of the other samples led to increased amounts of these side products, it is concluded that the ideal Ti/ Mo ratio is 4:5, and no noticeable phase range exists.

That $MoAs_2$ is isostructural with $NbSb_2$, whereas no "$MoSb_2$" is known, suggests that a phase range with different Ti/Mo ratios may exist in (Ti, Mo)As_2. Accordingly, a series of samples in this system were prepared with different Ti/Mo ratios, which were similarly heated in ceramic containers placed inside sealed silica tubes. The highest yields were obtained above 800 °C, and the samples with Ti/Mo ratios smaller than 0.9:1.1 appeared to be phase-pure. Attempts to replace Mo with W failed in both cases.

Analyses. Initial analyses were performed with an X-ray powder diffractometer with position-sensitive detector (INEL). The diffractogram of the antimonide was similar to that of $NbSb_2$. For the arsenides, the pattern obtained after reaction strongly resembled that of $MoAs_2$, although the peak positions in the powder X-ray diffractograms moved toward lower angles with increasing Ti content, indicative of an increase of the unit cell dimensions (Pauling radii are 1.32 Å for Ti and 1.29 Å for Mo[23]).

Subsequent EDS analyses (LEO 1530, with integrated EDAX Pegasus 1200) revealed no incorporation of impurity elements, such as oxygen or silicon stemming from the silica tube. The M/Pn (Pn = As, Sb) ratios of several selected crystals were averaged to 33:(67 ± 1) atom %. The Ti/Mo ratio was 44:(56 ± 1) atom % for the antimonide, which did not exhibit a phase range, and in the arsenides the ratio was consistently below 42:(58 ± 1) at.-% in various reaction products.

Single-Crystal Structure Studies. A black, block-shaped single crystal from the sample with a starting composition of "$Ti_4Mo_5Sb_{18}$" was mounted for a room-temperature single-crystal X-ray data collection on a Smart Apex CCD (BRUKER), which utilizes graphite-monochromatized Mo Kα radiation. Data were collected by scans of 0.3° in ω, for two blocks of 606 frames at $\phi = 0°$ and 60°. The exposure time was 60 s per frame. The data set was corrected for Lorentz and polarization effects. Absorption corrections were made on the basis of fitting a function to the empirical transmission surface as sampled by multiple equivalent measurements using SADABS.[24] Diffraction peaks obtained from all frames of the reciprocal space images were used to determine the unit cell parameters by a least-square analysis. For the structure refinements commencing from the $NbSb_2$ parameters, we employed the SHELXTL[25] program package. The one metal atom site, M, present in this structure of space group *C*2/*m* is mixed occupied by 39.7(5)% Ti and 60.3% Mo. No long-range ordering of the Ti and Mo atoms was found; i.e., refinement in the subgroups such as *Cm* resulted in two equivalently occupied M sites but revealed no ordering between the two.

Table 3. Selected Interatomic Distances (Å) of $Ti_{0.8}Mo_{1.2}Sb_4$ and $Ti_{0.9}Mo_{1.1}As_4$

distance	$Ti_{0.8}Mo_{1.2}Sb_4$	$Ti_{0.9}Mo_{1.1}As_4$
M−Pn1	2 × 2.8787(4)	2 × 2.645(2)
M−Pn1	2 × 2.8804(5)	2.688(2)
M−Pn1	2.9430(6)	2 × 2.700(2)
M−Pn2	2 × 2.7772(4)	2 × 2.567(2)
M−Pn2	2.8513(6)	2.602(2)
M−M	3.092(1)	2.992(3)
Pn2−Pn2	2.777(1)	2.461(3)
Pn2−Pn2	2 × 3.001(1)	2 × 2.754(2)

In the Ti/Mo/As system, no single crystal suitable for X-ray diffraction data collection was found. Therefore, Rietveld refinements were performed using the GSAS program.[26,27] The cell parameters and atomic positions were initially taken from $MoAs_2$ as the proposed model. A pseudo-Voigt peak shape profile, which is composed of both Gaussian and Lorentzian parameters, was chosen, and the parameters were refined to obtain the best fit to the experimental peak shapes (Figure 3). The M site is mixed occupied by 43(1)% Ti and 57% Mo. Again, no long-range ordering between cations was found. The crystallographic details and the atomic positions of both the antimonide and arsenide are summarized in Tables 1 and 2.

Electronic Structure Calculations. We performed self-consistent tight-binding LMTO calculations for the arsenide compound (LMTO = linear muffin tin orbitals)[28,29] In this method, the density-functional theory is applied with the local density approximation (LDA).[30] The integration in *k* space was carried out by an improved tetrahedron method.[31] The calculations were performed on hypothetical $TiMoAs_4$ and $TiMoSb_4$. Different possible Ti/Mo orderings were analyzed to investigate the electron density at the Fermi level.

Physical Property Measurements. Since no single crystals of sufficient dimensions were available, we pressed part of the samples into a bar-shaped pellet of the dimensions 6 mm × 2 mm × 1 mm for the temperature-dependent electrical resistance measurements using a four-point method. A homemade device was used to determine the voltage drops ΔV over a distance of 2 mm at a constant current of 2 mA under dynamic vacuum between 295 and 160 K, wherein cooling was achieved by helium compression. Silver paint (Ted Pella) was used to create the electric contacts.

The Seebeck coefficient *S* of the samples was determined on cold-pressed bars prepared by the same method. A commercial

(23) Pauling, L. *The Nature of the Chemical Bond*; Cornell University Press: Ithaca, NY, 1948.
(24) *SAINT*; Siemens Analytical X-ray Instruments, Inc.: Madison, WI, 1995.
(25) Sheldrick, G. M. *SHELXTL*; Siemens Analytical X-Ray Systems: Madison, WI, 1995.
(26) Larson, A. C.; Von Dreele, R. B. *General Structure Analysis System (GSAS)*; Los Alamos National Laboratory Report LA-UR-86-748, 2000.
(27) Toby, B. H. *J. Appl. Crystallogr.* **2001**, *34*, 210.
(28) Andersen, O. K. *Phys. Rev. B: Solid State* **1975**, *12*, 3060.
(29) Skriver, H. L. *The LMTO Method*; Springer-Verlag: Berlin, Germany, 1984.
(30) Hedin, L.; Lundqvist, B. I. *J. Phys. C: Solid State Phys.* **1971**, *4*, 2064.
(31) Blöchl, P. E.; Jepsen, O.; Andersen, O. K. *Phys. Rev. B: Condens. Matter* **1994**, *49*, 16223.

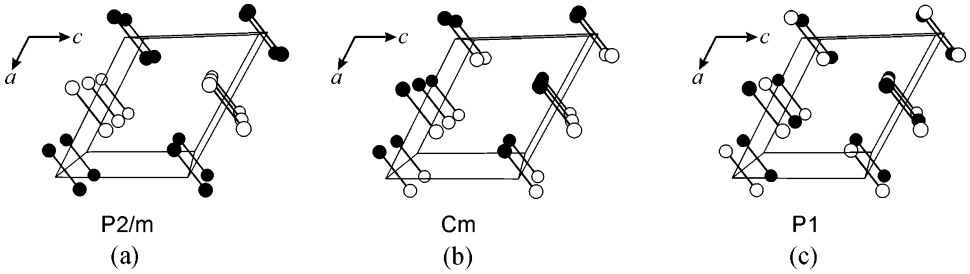

Figure 6. Three different possible M−M orderings with the corresponding space groups. For clarity, As/Sb atoms are removed.

thermopower measurement apparatus (MMR Technologies) was used to measure *S* under dynamic vacuum in the temperature range between 300 and 550 K, using constantan as an internal standard to determine the temperature difference and silver paint for the contacts.

Results and Discussion

Crystal Structure. Both compounds are isostructural with $NbSb_2$ ($OsGe_2$[32] type). The crystal structure of $NbSb_2$ (Figure 4) contains two crystallographically different Sb atoms. The Sb1 atoms do not participate in any considerable homonuclear bonding; the contacts along the *a*-axis (dashed lines) are longer than 3.3 Å. However, the Sb2 atoms form puckered layers (left layer in Figure 4) with one short Sb−Sb bond of 2.77 Å (thick lines in Figure 4) and two intermediate ones of 3.04 Å per Sb atom as emphasized via solid lines between the Sb atoms. In $Ti_{0.8}Mo_{1.2}Sb_4$, these distances are 2.78 and 3.00 Å, respectively, similar to $HfMoSb_4$ (2.79 and 3.06 Å).[22] Because of the different cations in these three antimonides, the unit cell volumes vary from 267.0 $Å^3$ ($NbSb_2$) to 258.4 $Å^3$ ($Ti_{0.8}Mo_{1.2}Sb_4$) and 273.9 $Å^3$ in $HfMoSb_4$. Considering these volume deviations, the shortest Sb−Sb bond is remarkably constant, between 2.77 and 2.79 Å and comparable to a typical single bond of 2.8 Å.[33,34] In $Ti_{0.9}Mo_{1.1}As_4$, the short As−As bond distance is 2.46 Å, and the longer one is 2.75 Å (Table 3).

The Nb atoms in $NbSb_2$ are located between the Sb atom layers in bicapped trigonal prismatic voids. Two Nb-centered prisms share one rectangular face, which leads to the formation of an Nb−Nb bond of 3.14 Å (Figure 5). Whereas this is significantly larger than a single bond of 2.9 Å, one may assign a d^1 configuration to the Nb atoms to a first approximation. In $Ti_{0.8}Mo_{1.2}Sb_4$ and $Ti_{09}Mo_{1.1}As_4$, the M−M bonds are 3.09 and 2.99 Å in length, respectively. Sb−Sb distances of 3.0−3.1 Å are often considered to have a bond order of $^1/_2$.[8,13,35] By the method of ignoring the Sb−Sb separation of >3.3 Å and treating the short Sb−Sb bond of 2.77 Å in $NbSb_2$ as a single bond and the longer ones as half bonds, the octet rule leads to $Nb^{4+}Sb^{-}Sb^{3-}$. However, as the Nb−Nb distance of 3.14 Å is much longer than a typical single bond, the counting scheme may only be a crude approximation. This electron counting scheme is just as valid for the isoelectronic $TiMoPn_4$ compounds as well, which leaves on average one d electron for each transition metal.

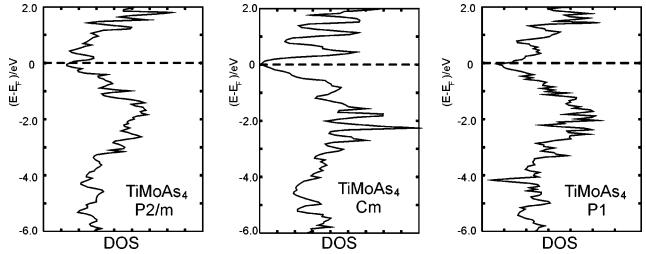

Figure 7. DOS for three proposed models of $TiMoAs_4$ with different Ti/Mo ordering. The horizontal dashed lines denote the Fermi levels, arbitarily placed at 0 eV.

However, the electron density is rather polarized along the Ti−Mo bonds.

Electronic Structure. Removing the *C* centering from the structure leads to the presence of only homonuclear M−M interactions, i.e., Ti−Ti and Mo−Mo, in the space group *P*2/*m* (Figure 6a). Alternatively, one can remove the 2-fold rotation axis, while the *C* centering is maintained. This model leads to the formation of heteronuclear Ti−Mo pairs within the space group *Cm* (Figure 6b). Finally, one can propose a model, where no symmetry (other than translational) exists; i.e., both *C* centering, mirror plane and 2-fold rotation axis are removed (space group *P*1 in Figure 6c).

The corresponding DOS of these models for $TiMoAs_4$ are compared in Figure 7. The differences in the total energies of these models are negligible. Only in the *Cm* model, where exclusively heteronuclear M−M bonds are present, the DOS at E_F are zero. A closer look at the actual band structure reveals that, such as for the corresponding $HfMoSb_4$ model, no bands are crossing E_F. It should be noted that these calculations are performed for the Ti/Mo ratio of 1. The Fermi level of $Ti_{0.9}Mo_{1.1}As_4$ would be located above the gap/local minimum, as Mo is more electron-rich than Ti. Therefore, this arsenide is predicted to be metallic independent of the actual short-range ordering. Because the calculated DOS of the antimonide (not shown) exhibit the same features, $Ti_{0.8}Mo_{1.2}Sb_4$ should be metallic as well. However, the occurrence of heteronuclear M−M interactions is likely preferred, as the related case of $HfMoSb_4$ shows.

Physical Properties. The experimentally determined specific electrical resistance is depicted in Figure 8. The curve is rather flat, most likely a consequence of the large grain boundary effect. The absolute value of 13 mΩ cm is typical for cold-pressed pellets of metallic materials. The measured Seebeck coefficient at 300 K in both the arsenide and the antimonide (Figure 8) is small, namely −7 μ and +10 μV/K, respectively. Such small values are typical for metals (≈10 μV/K for metals[1]).

(32) Weitz, G.; Born, L.; Hellner, E. *Z. Metallkd.* **1960**, *51*, 238.
(33) Hönle, W.; von Schnering, H.-G. *Z. Kristallogr.* **1981**, *155*, 307.
(34) Kleinke, H. *Chem. Commun.* **2000**, 1941.
(35) Popian, G. A.; Hoffman, R. *Angew. Chem., Int. Ed.* **2000**, *39*, 2408.

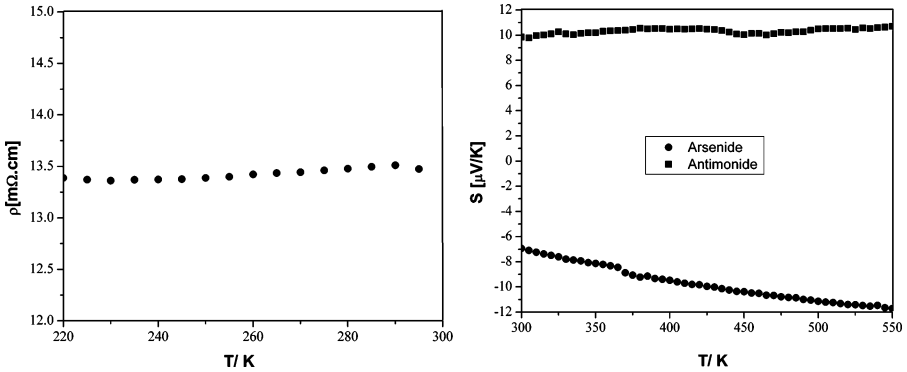

Figure 8. (left) Specific electrical resistance of $Ti_{0.9}Mo_{1.1}As_4$. (right) Seebeck coefficient of $Ti_{0.8}Mo_{1.2}As_4$ and $Ti_{0.9}Mo_{1.1}Sb_4$.

Conclusion

Two new ternary early transition metal pnictides, $Ti_{0.79(1)}Mo_{1.21}Sb_4$ and $Ti_{0.86(2)}Mo_{1.14}As_4$, were synthesized. Experimental evidence suggests that the former is a line compound (i.e., exhibits no noticeable phase range) and the latter exhibits a large phase range with $0.1 < \delta \leq 1$ in $Ti_{1-\delta}Mo_{1+\delta}As_4$. They both crystallize in the $OsGe_2$ type, space group *C*2/*m*. No long-range order, resulting in subgroups, was found to occur between the Ti and Mo atoms. $Ti_{0.79(1)}Mo_{1.21}Sb_4$ (≡(Ti,Mo)Sb_2) is unique in the respect that $TiSb_2$ forms a different type, and a "$MoSb_2$" is not known to exist. On the other hand, $MoAs_2$ crystallizes like $Ti_{0.86(2)}Mo_{1.14}As_4$ in the $OsGe_2$ type; hence, the ternary arsenide may be classified as a solid solution.

Electronic structure calculations for different ordered models of hypothetical $TiMoAs_4$ and $TiMoSb_4$ revealed that only the *Cm* models would be nonmetallic and thus of interest for the thermoelectric energy conversion. However, since these compounds exist only with Ti/Mo ratios <1, the Fermi level is located above the minimum in the DOS, and metallic behavior is expected regardless of the actual short-range Ti/Mo ordering. The physical properties of $Ti_{0.79(1)}Mo_{1.21}Sb_4$ and $Ti_{0.86(2)}Mo_{1.14}As_4$ are in accord with the predicted metallic behavior; hence, the thermoelectric properties are poor.

Thus far, $HfMoSb_4$ remains the only nonmetallic material in this family of pnictides forming the $OsGe_2$ type; therefore, our ongoing research focuses on optimizing the thermoelectric properties of $HfMoSb_4$ and finding other representatives, such as the hypothetical analogues *$ZrMoAs_4$*, *$HfMoAs_4$*, and *$ZrMoSb_4$*.

Acknowledgment. Financial support from NSERC, CFI, OIT (Ontario Distinguished Researcher Award for H.K.) and the Canada Research Chair program (CRC for H.K.) is appreciated.

Supporting Information Available: One X-ray crystallographic file (CIF). This material is available free of charge via the Internet at http://pubs.acs.org.

IC0619254